Large-scale symmetry-adapted perturbation theory computations via density fitting and Laplace transformation techniques: Investigating the fundamental forces of DNA-intercalator interactions

Edward G. Hohenstein, Robert M. Parrish, C. David Sherrill' , Justin M. Turney, and Henry F. Schaefer III

Citation: The Journal of Chemical Physics **135**, 174107 (2011); doi: 10.1063/1.3656681
View online: http://dx.doi.org/10.1063/1.3656681
View Table of Contents: http://aip.scitation.org/toc/jcp/135/17
Published by the American Institute of Physics

Large-scale symmetry-adapted perturbation theory computations via density fitting and Laplace transformation techniques: Investigating the fundamental forces of DNA-intercalator interactions

Edward G. Hohenstein,[1] Robert M. Parrish,[1] C. David Sherrill,[1,a)]
Justin M. Turney,[2] and Henry F. Schaefer III[2]
[1]*Center for Computational Molecular Science and Technology, School of Chemistry and Biochemistry, Georgia Institute of Technology, Atlanta, Georgia 30332-0400, USA*
[2]*Center for Computational Quantum Chemistry, Department of Chemistry, University of Georgia, Athens, Georgia 30602, USA*

(Received 9 August 2011; accepted 10 October 2011; published online 2 November 2011)

Symmetry-adapted perturbation theory (SAPT) provides a means of probing the fundamental nature of intermolecular interactions. Low-orders of SAPT (here, SAPT0) are especially attractive since they provide qualitative (sometimes quantitative) results while remaining tractable for large systems. The application of density fitting and Laplace transformation techniques to SAPT0 can significantly reduce the expense associated with these computations and make even larger systems accessible. We present new factorizations of the SAPT0 equations with density-fitted two-electron integrals and the first application of Laplace transformations of energy denominators to SAPT. The improved scalability of the DF-SAPT0 implementation allows it to be applied to systems with more than 200 atoms and 2800 basis functions. The Laplace-transformed energy denominators are compared to analogous partial Cholesky decompositions of the energy denominator tensor. Application of our new DF-SAPT0 program to the intercalation of DNA by proflavine has allowed us to determine the nature of the proflavine-DNA interaction. Overall, the proflavine-DNA interaction contains important contributions from both electrostatics and dispersion. The energetics of the intercalator interaction are are dominated by the stacking interactions (two-thirds of the total), but contain important contributions from the intercalator-backbone interactions. It is hypothesized that the geometry of the complex will be determined by the interactions of the intercalator with the backbone, because by shifting toward one side of the backbone, the intercalator can form two long hydrogen-bonding type interactions. The long-range interactions between the intercalator and the next-nearest base pairs appear to be negligible, justifying the use of truncated DNA models in computational studies of intercalation interaction energies. © *2011 American Institute of Physics*. [doi:10.1063/1.3656681]

I. INTRODUCTION

The characterization of noncovalent interactions is vital for the prediction of crystal structures and energetics,[1–4] understanding the structure of biological macromolecules,[5–14] and the study of drug binding to DNA and proteins.[15–22] Computationally, it is possible to obtain energetic and geometric information about noncovalent interactions as well as an analysis of the interaction in terms of physically meaningful components (i.e., electrostatics, exchange, induction, and dispersion).[23–28] Energy component analysis provides additional insight that can be used to develop better models of noncovalent interactions. The most rigorous means of obtaining such an analysis is through symmetry-adapted perturbation theory (SAPT),[27] which allows the interaction energy to be computed directly in terms of its physical components. Both wavefunction-based and density functional theory (DFT)-based formulations of SAPT are available; the most complete wavefunction-based SAPT approaches provide interaction energies of essentially coupled-cluster singles, doubles, and perturbative triples [CCSD(T)] quality.[27,29–33] In order to provide SAPT-based energy analyses for large, biological complexes, here we focus on the SAPT0 approach, which treats intermolecular interactions through second-order perturbation theory, and neglects intramonomer correlation. This method can provide qualitatively correct (and, at times, quantitatively correct) results for large systems (>200 atoms).[34]

The objective of this paper is to describe several new numerical techniques we have applied to the SAPT0 method to increase the maximum tractable system size by a factor of two, compared to our earlier work. Previously, we have applied density-fitting techniques to reduce the prefactor of the integral transformation in SAPT0,[34] and applied efficient density-fitting factorizations[35] and natural orbitals[36] to reduce the cost of including intramonomer correlation. This follows from previous work in the literature focused on applying efficient density-fitting factorizations to coupled Kohn-Sham DFT-based SAPT [SAPT(DFT)].[37–39] New techniques introduced here include efficient factorizations of all SAPT0 terms with density-fitted intermediates, the use of novel dressed three-index integrals to obviate the need for explicit formation of the dressed four-index two-electron integral (TEI)

a)Electronic mail: sherrill@gatech.edu.

tensor in the exchange terms, and the introduction of a Laplace transformation approach[40,41] using the quadratures of Braess and Hackbusch[42,43] to reduce much of the computational effort in the exchange-dispersion terms. These techniques allow the SAPT0 interaction energy to be evaluated with reduced $\mathcal{O}(N^3)$ disk storage and $\mathcal{O}(N^2)$ core memory, greatly increasing tractability. Moreover, the prefactor of the remaining $\mathcal{O}(N^5)$ steps is greatly diminished in this new SAPT0 implementation, markedly enhancing throughput. Finally, it should be noted that all of the techniques introduced here in the context of SAPT0 are immediately transferable to uncoupled-SAPT(DFT), and should allow for similar maximum tractable size improvements in the latter method. The more robust coupled-SAPT(DFT) method can also benefit from these factorizations (although separate techniques must be applied to the coupled dispersion term[37–39]); most importantly, the rate-limiting exchange-dispersion evaluation is identical in SAPT0 and SAPT(DFT) (see Eq. (10) of Ref. 39).

For a full description of the SAPT0 method, and as a starting point for the equations presented here, the reader should consult our previous paper on density fitting in SAPT0.[34] Below, we review the basics of SAPT, as well as the fundamental numerical techniques of density fitting of the TEI tensor[44–51] and Laplace transformation of the energy denominator.[40,41] Within the context of SAPT0, we then detail the application of specially dressed three-index integrals to provide an efficient density-fitted factorization of the induction term, and the concerted use of density-fitted integrals and Laplace decomposed energy denominators to significantly reduce the prefactor of the exchange-dispersion term. We then demonstrate the enhanced efficiency of the SAPT0 code by revisiting the linear acene timings of our first SAPT0 paper.[34] We also perform a benchmark study of the Laplace decomposition procedure over the S22 test set,[12] which is used to provide input parameters for quadrature cutoffs. This study also demonstrates a slight advantage of Laplace decomposition over the related pivoted Cholesky decomposition for the energy denominators.[52] Finally, we demonstrate the full utility of the new SAPT0 code by performing a systematic energy component analysis of the intermolecular interactions in a proflavine-DNA intercalator complex. These results indicate that the DNA backbone must be included to properly capture the physics of the intercalation process, due to hydrogen-bonding type interactions between the proflavine and the backbone. This conclusion demonstrates the need for a large-scale SAPT0 implementation. The SAPT0 computation of the full intercalator complex is the largest performed to date, with 220 atoms and 2845 basis functions.

The SAPT0 code presented here is implemented in the developers' version of the the open-source PSI4 package,[53] which is slated for public release at the end of 2011. In particular, density fitting is accomplished using three-index integrals from the new LIBMINTS library, written by one of the authors (J.M.T.). Although SAPT computations require multiple components (i.e., Hartree-Fock computations on the dimer and each monomer, plus the subsequent SAPT0 evaluation), the process is fully automated in the PSI4 PYTHON driver.[53]

II. THEORETICAL METHODS

A. Symmetry-adapted perturbation theory

In SAPT, the dimer Hamiltonian is partitioned into contributions from the Fock operator of each monomer (F), the interaction between the monomers (V), and the fluctuation potential of each monomer (W),

$$H = F_A + F_B + V + W_A + W_B. \tag{1}$$

The interaction energy can be written as a perturbation series,

$$E_{int} = \sum_{n=1}^{\infty}\sum_{k=0}^{\infty}\sum_{l=0}^{\infty}\left(E_{pol}^{(nkl)} + E_{exch}^{(nkl)}\right), \tag{2}$$

where n denotes the order in V, and k and l denote the order in W_A and W_B, respectively. Here, the E_{pol} terms originate from the *polarization expansion* and E_{exch} are repulsive terms resulting from the antisymmetry of the wavefunction with respect to the exchange of electrons between monomers. A more complete description of SAPT can be found in Ref. 27. The advantage of treating the interaction energy in this manner is that each term in Eq. (2) corresponds to a physical component of the interaction. This allows an energy component analysis of the interaction energy to be obtained simply by grouping the various SAPT terms. In this work, we will consider zeroth-order SAPT (SAPT0); terms through second-order in V and zeroth-order in W are included in the expansion

$$E_{SAPT0} = E_{elst}^{(10)} + E_{exch}^{(10)} + E_{ind,resp}^{(20)} + E_{exch-ind,resp}^{(20)} + \delta E_{HF} + E_{disp}^{(20)} + E_{exch-disp}^{(20)}, \tag{3}$$

where

$$\delta E_{HF}^{(2)} = E_{int}^{HF} - \left(E_{elst}^{(10)} + E_{exch}^{(10)} + E_{ind,resp}^{(20)} + E_{exch-ind,resp}^{(20)}\right). \tag{4}$$

Note that we compute the true $E_{exch}^{(10)}$ term instead of the simpler $E_{exch}^{(10)}(S^2)$ approximation throughout this work. The δE_{HF} term contains higher-order induction and exchange-induction interactions as well as some spurious exchange effects.[54,55] In practice, SAPT0 has been found to provide more accurate results when this term is included.[34]

The convention for the grouping of SAPT0 terms used in this work is as follows:

$$E_{elst} = E_{elst}^{(10)}, \tag{5}$$

$$E_{exch} = E_{exch}^{(10)}, \tag{6}$$

$$E_{ind} = E_{ind}^{(20)} + E_{exch-ind,resp}^{(20)} + \delta E_{HF}^{(2)}, \tag{7}$$

$$E_{disp} = E_{disp}^{(20)} + E_{exch-disp}^{(20)}. \tag{8}$$

Note again that the true infinite-order $E_{exch}^{(10)}$ term is computed.

All SAPT computations are performed using the developers' version of PSI4 (Ref. 53) and use Dunning's aug-cc-pVDZ and aug-cc-pVTZ basis sets.[56,57] Additionally, a truncated version of the aug-cc-pVDZ basis that lacks all diffuse functions on hydrogen atoms and diffuse d functions

on non-hydrogen atoms, denoted aug-cc-pVDZ′, is also used. The SAPT0/aug-cc-pVDZ′ level of theory has been found to exhibit fortuitous error cancellation between the overestimation of the uncoupled MP2-like dispersion treatment and the underestimation induced by basis set incompleteness error.[34]

B. Density fitting

One of the major computational difficulties encountered throughout quantum chemistry is the storage and manipulation of the four-index two-electron integral (TEI) tensor,

$$(\mu\nu|\lambda\sigma) = \iint_{\mathbb{R}^6} \phi_\mu(\vec{r}_1)\phi_\nu(\vec{r}_1)\frac{1}{r_{12}}\phi_\lambda(\vec{r}_2)\phi_\sigma(\vec{r}_2)\,\mathrm{d}r_1\,\mathrm{d}r_2, \tag{9}$$

which is seen here in the AO basis. Due to properties of the $1/r$ operator, this tensor is symmetric positive semidefinite and has only linear numerical rank, if written as the compound index matrix $I^{\lambda\sigma}_{\mu\nu}$. This fact is exploited in the related techniques of density fitting (DF)[44–51] and Choleksy decomposition (CD).[58–61] In the CD approach, the fully-pivoted partial Cholesky decomposition of the TEI tensor is directly obtained via the standard Cholesky decomposition algorithm, resulting in a factorization of the form,

$$(\mu\nu|\lambda\sigma) \approx L^Q_{\mu\nu}L^Q_{\lambda\sigma}, \tag{10}$$

where Q is the Cholesky vector index, which is analogous to the auxiliary basis dimension of the DF approach. Here and throughout this paper, the generalized Einstein convention is used, in which summations are implied over repeated indices occurring on only one side of the equation. Unfortunately, practical formation of the Cholesky decomposition requires that the entire $L^Q_{\mu\nu}$ tensor be held in core, significantly limiting the size of system that may be studied. Therefore, we have elected to pursue the alternative DF approach, which shares many similarities with CD, but may be efficiently performed out-of-core.

In the DF approach, also referred to as resolution of the identity (RI), the one-electron products of the type $\phi_\mu(\vec{r})\phi_\nu(\vec{r})$ in the bra and ket of the TEI tensor are fitted to a set of auxiliary basis functions $\chi_A(\vec{r})$. The fitting is typically performed by minimizing the sum-of-squares error in the electric field, though many other metrics have been proposed. If the electric field metric is used, the TEI tensor is decomposed as

$$(\mu\nu|\lambda\sigma) \approx (\mu\nu|A)[J_{AB}]^{-1}(B|\lambda\sigma), \tag{11}$$

where the raw three-index tensor $(\mu\nu|A)$ is

$$(\mu\nu|A) = \iint_{\mathbb{R}^6} \phi_\mu(\vec{r}_1)\phi_\nu(\vec{r}_1)\frac{1}{r_{12}}\chi_A(\vec{r}_2)\,\mathrm{d}r_1\,\mathrm{d}r_2, \tag{12}$$

and the two-index fitting metric J_{AB} is

$$J_{AB} = \int\int_{\mathbb{R}^6} \chi_A(\vec{r}_1)\frac{1}{r_{12}}\chi_B(\vec{r}_2)\,\mathrm{d}r_1\,\mathrm{d}r_2. \tag{13}$$

A key feature of using the decomposition of Eq. (11) is the reduction of integral generation and tensor storage and I/O costs from $\mathcal{O}(N^4)$ to $\mathcal{O}(N^3)$. Moreover, the decomposition of the four-index TEI tensor into a product of two- and three-index tensors often allows for serendipitous factorization of contractions of the TEI tensor, which can provide significant scaling and/or prefactor reduction. It should be noted that the most commonly cited disadvantage of the DF approach is that the auxiliary basis $\{\chi_A\}$ must be carefully preoptimized to fit primary basis function pairs. However, for the Dunning correlation-consistent bases, much work has been performed by Weigend to provide robust auxiliary basis sets for fitting Coulomb- and exchange-type integrals (the -JKFIT sets),[50] and ov (occupied · virtual) type integrals (the -RI sets).[62] These auxiliary bases contain 4–5 N functions for double-zeta bases, and 2–3 N functions for pentuple-zeta bases, where N is the number of primary basis functions, implying that the DF approach should be increasingly efficient for larger basis sets.

In practice, a symmetric three-index tensor $C^Q_{\lambda\sigma}$ is often used,

$$(\mu\nu|\lambda\sigma) \approx (\mu\nu|A)[J_{AQ}]^{-1/2}[J_{QB}]^{-1/2}(B|\lambda\sigma) = C^Q_{\mu\nu}C^Q_{\lambda\sigma}. \tag{14}$$

The $C^Q_{\mu\nu}$ tensor is analogous to the $L^Q_{\mu\nu}$ tensor of CD, implying that DF and CD are practically indistinguishable once these tensors are built.

In SAPT, the TEI tensor for both monomers must be built in the molecular orbital basis. This integral transformation step, which conventionally scales as $\mathcal{O}(N^5)$, can be reduced to $\mathcal{O}(N^4)$ by transforming the DF three-index tensors; for example, for the monomer A ov block,

$$C^Q_{a_1\nu} = C_{\mu a_1}C^Q_{\mu\nu}, \tag{15}$$

$$C^Q_{a_1r_1} = C_{\nu r_1}C^Q_{a_1\nu},$$

where $C_{\mu a_1}$ and $C_{\mu r_1}$ are the occupied and virtual portions of the monomer A SCF coefficient matrix, respectively. In this work, i, j, k, l are used to index any molecular orbital, a, b are used to index occupied molecular orbitals of monomer A and B, respectively, and r, s index virtual molecular orbitals of monomer A and B, respectively. If only the ov and/or oo blocks are required, additional prefactor gain can be realized by performing the contraction with the inverse square root of the fitting metric *after* performing the AO to MO transformation on the raw three-index tensor; this is commonly employed in DF-MP2. However, the induction term of SAPT0 requires the vv block of the TEI tensor, and, moreover, two complete sets of MO-basis DF integrals are required. For these reasons, we perform the symmetric fitting of the raw three-index tensor immediately, and subsequently perform the AO to MO transformations for the two monomers. We also retain the permutational symmetry in the large vv integral block to reduce disk I/O by a factor of two.

A note of caution, echoed here from the SAPT(DFT) work of Hesselmann *et al.*,[38] is appropriate regarding the choice of auxiliary basis for various SAPT terms. The -JKFIT sets are designed to fit the electrostatic and exchange terms (as in Hartree-Fock), while the -RI sets are more appropriate for monomer density changes at valence length-scales due to induction or dispersion. For first-row and (for the most part) second-row elements, these two fitting bases may be used interchangeably for all SAPT0 terms with negligible error. However, for third-row and deeper elements, the -RI sets are notably lacking in ability to fit core electrons, which manifests

as large fitting errors in the electrostatic term if an -RI set is used. However, induction and dispersion terms appear to be quite robust against this error. For these reasons, it is recommended to use the -JKFIT bases to evaluate the electrostatic and exchange terms, and use the -RI bases for all others. This is possible in our PSI4 SAPT implementation, and it leads to a negligible increase in computation time.

C. Laplace transform techniques

Perturbation theory is plagued with the presence of nonlinear energy denominator tensors, which require explicit and expensive evaluation of numerator elements prior to summation into the energy. For the dispersion and exchange-dispersion terms of SAPT0, the specific denominator tensor is

$$\Delta_{a_1 r_1}^{b_1 s_1} = \frac{1}{\epsilon_{r_1} + \epsilon_{s_1} - \epsilon_{a_1} - \epsilon_{b_1}}, \tag{16}$$

where ϵ_{r_1} and ϵ_{s_1} are virtual orbital eigenvalues, and ϵ_{a_1} and ϵ_{b_1} are occupied orbital eigenvalues, for monomers A and B, respectively. If the concatenated sets of orbital eigenvalues $\{c_1\}$ and $\{d_1\}$ are made by combining monomer eigenvalues as $\{a_1, b_1\}$ and $\{r_1, s_1\}$, the SAPT0 energy denominator may be viewed as an off-diagonal block of the augmented energy denominator tensor,

$$\Theta_{c_1 d_1}^{c_2 d_2} = \frac{1}{\epsilon_{d_1} + \epsilon_{d_2} - \epsilon_{c_1} - \epsilon_{c_2}}. \tag{17}$$

This tensor is symmetric positive semidefinite, and has been shown to be of *constant* numerical rank, regardless of the system size or nature of the electronic environment.[43] This was first recognized and exploited by Almlöf, who proposed the Laplace decomposition technique for energy denominators,[40,41] and Koch, who proposed the Cholesky decomposition procedures for energy denominators.[52] In the more intuitive Cholesky decomposition approach, the fully-pivoted partial Cholesky decomposition is directly sought, which typically converges to a maximum Chebyshev error of 1×10^{-6} or less in 6–10 Cholesky vectors, and provides the factorization,

$$\Theta_{c_1 d_1}^{c_2 d_2} \approx \sigma_{c_1 d_1}^{w} \sigma_{c_2 d_2}^{w}, \tag{18}$$

where w is the constant-scaling Cholesky vector index. Remarkably, an analytic, i.e., non-recursive Cholesky decomposition formula is available for the particular functional form of the energy denominator.[52] Alternatively, the Laplace decomposition of the Heaviside step function $1(t)$ provides the serendipitous result,

$$\mathcal{L}\{1(t)\} = \int_0^{+\infty} \exp(-xt)\, \mathrm{d}t = \frac{1}{x}. \tag{19}$$

The indefinite integral in the Laplace transformation may be evaluated by numerical quadrature as

$$\frac{1}{x} \approx \sum_w \alpha_w \exp(-x t_w), \tag{20}$$

which, when applied in the context of energy denominators, gives

$$\Theta_{c_1 d_1}^{c_2 d_2} \approx \tau_{c_1}^{w} \tau_{d_1}^{w} \tau_{c_2}^{w} \tau_{d_2}^{w}, \tag{21}$$

where $\tau_{c_1}^2 = \sqrt[4]{\alpha_w} \exp(\epsilon_{c_1} t_w)$ and $\tau_{d_1} = \sqrt[4]{\alpha_w} \exp(-\epsilon_{d_1} t_w)$, which requires positive definite quadrature weights. This formula has enhanced flexibility relative to the Cholesky decomposition; however, this flexibility cannot be exploited when Laplace decomposition is used in concert with density fitting. Therefore, we will group pairs of orbital indices, and approximate the denominator tensor as

$$\Theta_{c_1 d_1}^{c_2 d_2} \approx \pi_{c_1 d_1}^{w} \pi_{c_2 d_2}^{w}, \tag{22}$$

where $\pi_{c_1 d_1}^{w} = \sqrt{\alpha_w} \exp(-(\epsilon_{d_1} - \epsilon_{c_1}) t_w)$.

The choice of quadrature is critically important for the efficiency of the Laplace decomposition procedure. Naïve Chebyshev or Gauss-Laguerre quadratures are unsuitable, often requiring dozens of quadrature points for μH accuracy. However, many more advanced quadratures for the particular problem of energy denominators have been developed over the past two decades. The first advancement was proposed by Almlöf and involves directly minimizing the sum-of-squares error of the quadrature with respect to a metric describing the frequency and importance of values in the denominator tensor for a particular molecular problem.[41] The second advancement was proposed by Hackbusch, who completely abandons the particulars of the molecular problem, and instead optimizes the Chebyshev norm of the error over the intrinsic range of the problem by the minimax algorithm.[42,43] The intrinsic range R is simply stated as

$$R = \frac{\epsilon_{\mathrm{HUMO}} - \epsilon_{\mathrm{LOMO}}}{\epsilon_{\mathrm{HOMO}} - \epsilon_{\mathrm{LUMO}}}, \tag{23}$$

where HUMO denotes the highest active unoccupied orbital, LOMO denotes the lowest active occupied orbital, LUMO denotes the lowest active unoccupied orbital, and HOMO denotes the highest active occupied orbital. While this technique initially appears to be strongly dependent on the electronic environment (e.g., a low-bandgap system will necessarily have more quadrature points), the convergence of the quadrature is exponential regardless of the intrinsic range, resulting in a constant number of required vectors for *all* problems. Moreover, pivoted Cholesky decomposition shows a similar constant increase in required vectors in low-bandgap systems. Hackbusch has kindly made his quadratures available to the community (see www.mis.mpg.de/scicomp/EXP_SUM/1_x/), and we have adopted their use in the PSI4 program. In our comparisons of Cholesky and Laplace decomposition techniques, we find that both methods produce extremely efficient decompositions of the energy denominator, with ~6–10 points required for μH accuracy in the denominator, depending on the intrinsic size of the problem. A more thorough comparison between Laplace and Cholesky decompositions of SAPT0 energy denominators is presented in the "Results and Discussion" section.

In the context of SAPT, error need only be minimized in the off-diagonal intermonomer block of the augmented energy denominator tensor. This fact can be trivially exploited to slightly increase the efficiency of Laplace-

or Cholesky-decomposed SAPT denominators for heterogeneous monomers. In SAPT Laplace decomposition, Eq. (23) may be modified to give the effective intrinsic range,

$$R' = \frac{\epsilon^A_{\mathrm{HUMO}} + \epsilon^B_{\mathrm{HUMO}} - \epsilon^A_{\mathrm{LOMO}} - \epsilon^B_{\mathrm{LOMO}}}{\epsilon^A_{\mathrm{LUMO}} + \epsilon^B_{\mathrm{LUMO}} - \epsilon^A_{\mathrm{HOMO}} - \epsilon^B_{\mathrm{HOMO}}}. \tag{24}$$

In a supermolecular pivoted Cholesky decomposition approach, the algorithm is terminated when the maximum element on the diagonal of the residual matrix D falls below the desired error criteria δ,

$$\max \sqrt{D_{kk} D_{kk}} < \delta. \tag{25}$$

The off-diagonal elements are all guaranteed to be of equal or smaller magnitude than the maximum diagonal element, or else a 2×2 minor would be able to be extracted with a negative determinant, in violation of the positive semidefiniteness of the tensor. In SAPT, the desired accuracy need only be guaranteed in the intermonomer block, so the termination criteria may be relaxed to

$$\max \sqrt{D^A_{kk} D^B_{ll}} < \delta. \tag{26}$$

The utility of a concerted DF and Laplace transform approach is easily understood in terms of the SAPT0 dispersion energy, which is completely analogous to the opposite-spin term in MP2,[63]

$$E^{(20)}_{disp} = -4 \frac{(a_1 r_1 | b_1 s_1)(a_1 r_1 | b_1 s_1)}{\epsilon_{r_1} + \epsilon_{s_1} - \epsilon_{a_1} - \epsilon_{b_1}}. \tag{27}$$

The computational cost of this term is determinated by the $\mathcal{O}(oN^4)$ integral transformation. Using DF techniques alone, the prefactor is reduced to $\mathcal{O}(o^2 v^2 N_{aux})$, but the scaling is untouched, as the full TEI tensor in the numerator must be formed. However, applying DF and Laplace transforms together results in

$$E^{(20)}_{disp} \approx -4 \pi^w_{a_1 r_1} \pi^w_{b_1 s_1} C^Q_{a_1 r_1} C^Q_{b_1 s_1} C^R_{a_1 r_1} C^R_{b_1 s_1}, \tag{28}$$

which may be factored to

$$\begin{aligned} Y^w_{QR} &= \pi^w_{a_1 r_1} C^Q_{a_1 r_1} C^R_{a_1 r_1}, \\ Z^w_{QR} &= \pi^w_{b_1 s_1} C^Q_{b_1 s_1} C^R_{b_1 s_1}, \\ E^{20}_{disp} &\approx -4 Y^w_{QR} Z^w_{QR}, \end{aligned} \tag{29}$$

which scales as $\mathcal{O}(ovN^2_{aux} N_w) \propto \mathcal{O}(N^4)$, because N_w is of order unity. In practice, the exact (within the DF approximation) $E^{(20)}_{disp}$ term is actually obtained for free as a byproduct of the few $E^{(20)}_{exch-disp}$ terms which cannot be factored to $\mathcal{O}(N^4)$. However, these Laplace transform techniques are used to factor most of the $E^{(20)}_{exch-disp}$ terms to $\mathcal{O}(N^4)$, greatly reducing the prefactor of this term. The specifics of which terms utilitize Laplace transform techniques is discussed below.

D. Generalized two-electron integrals

The exchange terms in SAPT present unique challenges for the introduction of DF integrals. The exchange interactions can be formulated in terms of second-quantization or interaction density matrices.[64,65] The second-quantization approach leads to equations which depend only on Coulomb type two-electron integrals [$(AA|BB)$, where $A(B)$ refers to any index on monomer A (B)] and are amenable to the introduction of DF integrals.[35] The interaction density matrix approach leads to more complex equations that include Coulomb, exchange [$(AB|AB)$], and hybrid [$(AA|AB)$] integrals. This approach involves integrals with fewer virtual indices than the second-quantization approach. Subsequently, the exchange corrections derived with the interaction density matrix approach have a lower computational scaling. However, the interaction density matrix approach uses generalized (dressed) two-electron integrals rather than the bare two-electron integrals found in the second-quantization approach. The generalized two-electron integrals are given as[66]

$$\tilde{v}^{jl}_{ik} = v^{jl}_{ik} + (i|j) \frac{(k|v_A|l)}{N_A} + (k|l) \frac{(i|v_B|j)}{N_B} + (i|j)(k|l) \frac{V_0}{N_A N_B}, \tag{30}$$

where $v^{jl}_{ik} = (ij|kl)$, $(i|j)$ are molecular overlap integrals, $(i|v|j)$ are nuclear attraction integrals (corresponding to the nuclei of one monomer), and V_0 is the intermolecular nuclear repulsion energy.

Under the DF approximation, the generalized two-electron integrals are written as

$$\begin{aligned} \tilde{v}^{jl}_{ik} \approx\ & C^P_{ij} C^P_{kl} + (i|j) \frac{(k|v_A|l)}{N_A} + (k|l) \frac{(i|v_B|j)}{N_B} \\ & + (i|j)(k|l) \frac{V_0}{N_A N_B}. \end{aligned} \tag{31}$$

Our initial implementation of DF-SAPT evaluated generalized two-electron integrals as shown above; the approximate four-index integrals were formed and then dressed with one-electron contributions. However, it is possible to define DF intermediates that include the one-electron contributions by adding three additional entries to the auxiliary index,

$$\begin{aligned} A^1_{ij} &= C^1_{ij}, \\ &\vdots \\ A^{N_{df}}_{ij} &= C^{N_{df}}_{ij}, \\ A^{N_{df}+1}_{ij} &= (i|j), \\ A^{N_{df}+2}_{ij} &= \frac{(i|v_B|j)}{N_B}, \\ A^{N_{df}+3}_{ij} &= (i|j) \sqrt{\frac{V_0}{N_A N_B}}, \end{aligned} \tag{32}$$

and

$$\begin{aligned} B^1_{ij} &= C^1_{ij}, \\ &\vdots \\ B^{N_{df}}_{ij} &= C^{N_{df}}_{ij}, \\ B^{N_{df}+1}_{ij} &= \frac{(i|v_A|j)}{N_A}, \\ B^{N_{df}+2}_{ij} &= (i|j), \\ B^{N_{df}+3}_{ij} &= (i|j) \sqrt{\frac{V_0}{N_A N_B}}. \end{aligned} \tag{33}$$

Now, the length of the auxiliary index is equal to the number of DF basis functions plus three ($n_{aux} = n_{df} + 3$). This allows the generalized two-electron integrals to be formed directly as

$$\tilde{v}_{ik}^{jl} \approx A_{ij}^{P} B_{kl}^{P}. \tag{34}$$

In practice, the A and B quantities are not explicitly stored; rather, the C type DF integrals are stored and the three additional auxiliary indices are appended as necessary when these integrals are read into memory. The memory requirements for the DF integrals needed to evaluate Eq. (34) for two-electron integrals with bra-ket symmetry [i.e., $(ij|ij)$ type integrals] would be, in principle, doubled. However, in practice, this doubling is only encountered for $(ab|ab)$ integrals, where the $o^2 n_{aux}$ DF integrals can easily be stored in memory. The $(as|as)$ and $(rb|rb)$ integrals appear in higher-order corrections not considered here. Even in those cases, these integrals appear only once, and the symmetry of the DF integrals cannot be exploited in the most efficient factorization of those exchange terms. Finally, the $(rs|rs)$ two-electron integrals do not appear in the SAPT exchange corrections. Therefore, the potential loss of symmetry in the formation of generalized two-electron integrals is not a problem.

To illustrate the utility of the three-index representation of generalized two-electron integrals, we will consider the $E_{exch}^{(10)}(S^2)$ term. Note that the use of the S^2 approximation is only for sake of example; the factorization of the true infinite-order $E_{exch}^{(10)}$ term follows immediately from this treatment, and is used in all computations in this study. The leading exchange term, under the S^2 approximation, is given by[66]

$$\begin{aligned} E_{exch}^{(10)}(S^2) = &-2\tilde{v}_{a_1 b_1}^{b_1 a_1} - 2S_{a_2}^{b_1}\left(2\tilde{v}_{a_1 b_1}^{a_1 a_2} - \tilde{v}_{a_1 b_1}^{a_2 a_1}\right) \\ &- 2S_{b_2}^{a_1}\left(2\tilde{v}_{a_1 b_1}^{b_2 b_1} - \tilde{v}_{a_1 b_1}^{b_1 b_2}\right) + 4S_{a_2}^{b_1} S_{b_2}^{a_2} \tilde{v}_{a_1 b_1}^{a_1 b_2} \\ &+ 4S_{a_2}^{b_2} S_{b_2}^{a_1} \tilde{v}_{a_1 b_1}^{a_2 b_1} - 2S_{a_2}^{b_1} S_{b_2}^{a_1} \tilde{v}_{a_1 b_1}^{a_2 b_2}, \end{aligned} \tag{35}$$

where S is the matrix of overlap integrals. The $E_{exch}^{(10)}(S^2)$ term can be rewritten in terms of generalized DF integrals and a few simple intermediates,

$$\tilde{a}^{P} = A_{a_1 a_1}^{P}, \tag{36}$$

$$\tilde{b}^{P} = B_{b_1 b_1}^{P}, \tag{37}$$

$$X_{b_1 b_2} = S_{a_2}^{b_1} S_{b_2}^{a_2}, \tag{38}$$

$$X_{a_1 a_2} = S_{a_2}^{b_2} S_{b_2}^{a_1}, \tag{39}$$

in a form that can be efficiently implemented without forming four-index arrays.

$$\begin{aligned} E_{exch}^{(10)}(S^2) = &-2A_{a_1 b_1}^{P} B_{a_1 b_1}^{P} - 2S_{a_2}^{b_1}\left(2\tilde{a}^{P} B_{a_2 b_1}^{P} - A_{a_1 a_2}^{P} B_{a_1 b_1}^{P}\right) \\ &- 2S_{b_2}^{a_1}\left(2A_{a_1 b_2}^{P}\tilde{b}^{P} - A_{a_1 b_1}^{P} B_{b_1 b_2}^{P}\right) + 4X_{b_1 b_2}\tilde{a}^{P} B_{b_1 b_2}^{P} \\ &+ 4X_{a_1 a_2} A_{a_1 a_2}^{P}\tilde{b}^{P} - 2S_{a_2}^{b_1} S_{b_2}^{a_1} A_{a_1 a_2}^{P} B_{b_1 b_2}^{P}. \end{aligned} \tag{40}$$

This formulation of the $E_{exch}^{(10)}(S^2)$ term allows for a memory efficient implementation by blocking over the P index.

E. Coupled-perturbed Hartree-Fock equations

The leading induction term contains two contributions: the changes to the electron density of monomer A induced by monomer B's electrostatic potential and the changes to the electron density of monomer B induced by monomer A's electrostatic potential. Through second-order in V, these changes are not coupled to each other,[66]

$$\begin{aligned} E_{ind,r}^{(20)}(A \leftarrow B) &= 2s_{a_1}^{r_1}(\omega_B)_{a_1}^{r_1}, \\ E_{ind,r}^{(20)}(B \leftarrow A) &= 2s_{b_1}^{s_1}(\omega_A)_{s_1}^{b_1}. \end{aligned} \tag{41}$$

This term can be evaluated with or without orbital response; the difference is the origin of the s coefficients. Here, we will discuss only the more rigorous formulation that includes the effect of orbital response. In this case, $s_{a_1}^{r_1}$ and $s_{b_1}^{s_1}$ are solutions to the Coupled-perturbed Hartree-Fock (CPHF) equations for their corresponding monomer. Obviously, the work associated with the evaluation of this correction is entirely in the solution of the CPHF equations,

$$s_{a_1}^{r_1} = \left(\left[4v_{r_1 r_2}^{a_1 a_2} - v_{r_1 r_2}^{a_2 a_1} - v_{a_2 r_2}^{a_1 r_1}\right]s_{a_1}^{r_1} + (\omega_B)_{a_1}^{r_1}\right)/(\epsilon_{a_1} - \epsilon_{r_1}). \tag{42}$$

It should be noted that these equations can be solved non-iteratively as a linear system of equations; however, this would scale as $\mathcal{O}(o^3 v^3)$. The iterative solution of these equations scales $\mathcal{O}(o^2 v^2)$, although the formation of the required matrix will scale $\mathcal{O}(N^5)$ [the exact scaling is dependent on the algorithm; under the DF approximation, the scaling is $\mathcal{O}(o^2 v^2 N_{df})$]. To avoid the $\mathcal{O}(N^5)$ step and its associated storage requirements, the DF representation of the two-electron integrals is introduced and the multiplication by s is distributed,

$$\begin{aligned} s_{a_1}^{r_1} = \big(&4C_{a_1 r_1}^{P} C_{a_2 r_2}^{P} s_{a_2}^{r_2} - C_{a_2 r_1}^{P} C_{a_1 r_2}^{P} s_{a_2}^{r_2} - C_{a_1 a_2}^{P} C_{r_1 r_2}^{P} s_{a_2}^{r_2} \\ &+ (\omega_B)_{a_1}^{r_1}\big)/(\epsilon_{a_1} - \epsilon_{r_1}). \end{aligned} \tag{43}$$

This allows contributions from $v_{r_1 r_2}^{a_1 a_2} s_{a_1}^{r_1}$ to be evaluated as $\mathcal{O}(ovN_{df})$, $v_{r_1 r_2}^{a_2 a_1} s_{a_1}^{r_1}$ as $\mathcal{O}(o^2 v N_{df})$, and $v_{a_2 r_2}^{a_1 r_1} s_{a_1}^{r_1}$ as $\mathcal{O}(ov^2 N_{df})$. The bottleneck associated with this implementation is the disk I/O associated with the $C_{r_1 r_2}^{P} s_{a_2}^{r_2}$ contraction. To improve efficiency, the two-fold permutational symmetry of the $C_{r_1 r_2}^{P}$ DF integrals is exploited in their storage. A similar algorithm that has been generalized for the solution of the coupled-perturbed Kohn-Sham equations (with and without the inclusion of Hartree-Fock exchange) can be found in Ref. 39.

F. Exchange-dispersion evaluation

The $E_{exch-disp}^{(20)}$ evaluation is the most computationally demanding portion of a SAPT0 computation. Under the approximations considered, it is the only SAPT0 term that unavoidably scales $\mathcal{O}(N^5)$. First, we will consider the canonical form of this correction:[67]

$$\begin{aligned} E_{exch-disp}^{(20)}(S^2) = &-2t_{r_1 s_1}^{a_1 b_1}\left[\tilde{v}_{a_1 b_1}^{s_1 r_1} + S_{a_1}^{s_1}\left(2\tilde{v}_{a_2 b_1}^{a_2 r_1} - \tilde{v}_{a_2 b_1}^{r_1 a_2}\right)\right. \\ &+ S_{a_2}^{s_1}\left(2\tilde{v}_{a_1 b_1}^{r_1 a_2} - \tilde{v}_{a_1 b_1}^{a_2 r_1}\right) + S_{b_1}^{r_1}\left(2\tilde{v}_{a_1 b_2}^{s_1 b_2} - \tilde{v}_{a_1 b_2}^{b_2 s_1}\right) \\ &+ S_{b_2}^{r_1}\left(2\tilde{v}_{a_1 b_1}^{b_2 s_1} - \tilde{v}_{a_1 b_1}^{s_1 b_2}\right) + S_{b_1}^{r_1} S_{a_2}^{b_2}\tilde{v}_{a_1 b_2}^{a_2 s_1} \\ &- 2S_{b_2}^{r_1} S_{a_2}^{b_2}\tilde{v}_{a_1 b_1}^{a_2 s_1} - 2S_{b_1}^{r_1} S_{a_1}^{b_2}\tilde{v}_{a_2 b_2}^{a_2 s_1} + 4S_{b_2}^{r_1} S_{a_1}^{b_2}\tilde{v}_{a_2 b_1}^{a_2 s_1} \end{aligned}$$

$$+ S^{s_1}_{a_1} S^{a_2}_{b_2} \tilde{v}^{r_1 b_2}_{a_2 b_1} - 2S^{s_1}_{a_2} S^{a_2}_{b_2} \tilde{v}^{r_1 b_2}_{a_1 b_1} - 2S^{s_1}_{a_1} S^{a_2}_{b_1} \tilde{v}^{r_1 b_2}_{a_2 b_2}$$
$$+ 4S^{s_1}_{a_2} S^{a_2}_{b_1} \tilde{v}^{r_1 b_2}_{a_1 b_2} + S^{r_1}_{b_2} S^{s_1}_{a_2} \tilde{v}^{a_2 b_2}_{a_1 b_1} - 2S^{r_1}_{b_1} S^{s_1}_{a_2} \tilde{v}^{a_2 b_2}_{a_1 b_2}$$
$$- 2S^{r_1}_{b_2} S^{s_1}_{a_1} \tilde{v}^{a_2 b_2}_{a_2 b_1} + S^{a_2}_{b_1} S^{b_2}_{a_1} \tilde{v}^{r_1 s_1}_{a_2 b_2} - 2S^{a_2}_{b_1} S^{b_2}_{a_2} \tilde{v}^{r_1 s_1}_{a_1 b_2}$$
$$- 2S^{a_2}_{b_2} S^{b_2}_{a_1} \tilde{v}^{r_1 s_1}_{a_2 b_1} \Big]. \quad (44)$$

As written above, this term can be implemented with $\mathcal{O}(o^3v^2)$ scaling. Heßelmann *et al.* propose a $\mathcal{O}(o^2v^2N_{df})$ factorization of the $t^{a_1 b_1}_{r_1 s_1} S^{a_2}_{b_1} S^{b_2}_{a_1} \tilde{v}^{r_1 s_1}_{a_2 b_2}$ term that uses DF integrals.[38] It is also possible to use a $\mathcal{O}(o^4v^2)$ algorithm to evaluate some of these terms; for small systems, the $\mathcal{O}(N^6)$ algorithm is competitive with the others, and for large basis sets, it can be superior to the DF factorization.

To find the optimal factorization of the $E^{(20)}_{exch-disp}$ term, we will examine each term separately and group similar terms together. First, we will look at the terms that unavoidably scale, with DF integrals and Laplace transformed energy denominators, as $\mathcal{O}(N^5)$,

$$E^{(20)}_{exch-disp}(S^2)(N^5) = -2t^{a_1 b_1}_{r_1 s_1} \Big[\tilde{v}^{s_1 r_1}_{a_1 b_1} - S^{s_1}_{a_2} \tilde{v}^{a_2 r_1}_{a_1 b_1} - S^{r_1}_{b_2} \tilde{v}^{s_1 b_2}_{a_1 b_1}$$
$$+ S^{r_1}_{b_2} S^{s_1}_{a_2} \tilde{v}^{a_2 b_2}_{a_1 b_1} + S^{a_2}_{b_1} S^{b_2}_{a_1} \tilde{v}^{r_1 s_1}_{a_2 b_2} \Big]. \quad (45)$$

Due to the exchange integrals that appear in this expression, the use of Laplace transformed energy denominators does not lead to any computational savings. The introduction of DF integrals, however, is helpful. First we will define a few simple intermediates as follows:

$$X^P_{a_1 s_1} = S^{s_1}_{a_2} A^P_{a_1 a_2},$$
$$X^P_{b_1 r_1} = S^{r_1}_{b_2} B^P_{b_1 b_2},$$
$$Y^P_{a_1 s_1} = S^{b_2}_{a_1} C^P_{b_2 s_1},$$
$$Y^P_{b_1 r_1} = S^{a_2}_{b_1} C^P_{a_2 r_1}. \quad (46)$$

This allows us to rewrite these $\mathcal{O}(N^5)$ terms in a particularly simple form

$$E^{(20)}_{exch-disp}(S^2)(N^5) = -2t^{a_1 b_1}_{r_1 s_1} \big(A^P_{a_1 s_1} - X^P_{a_1 s_1} \big) \big(B^P_{b_1 r_1} - X^P_{b_1 r_1} \big).$$
$$- 2t^{a_1 b_1}_{r_1 s_1} Y^P_{a_1 s_1} Y^P_{b_1 r_1}. \quad (47)$$

With this factorization, the contributions from these five terms can be evaluated with three $\mathcal{O}(o^2v^2N_{df})$ multiplications. The dispersion amplitudes do need to be formed, but they do not need to be stored. As a byproduct of this procedure, the $E^{(20)}_{disp}$ term can be obtained without any additional work.

While the Laplace transformed energy denominators do not help with all of the $E^{(20)}_{exch-disp}$ terms, they can reduce the scaling of some of the terms,

$$E^{(20)}_{exch-disp}(S^2)(\mathcal{L}) = -2t^{a_1 b_1}_{r_1 s_1} \Big[2S^{s_1}_{a_2} \tilde{v}^{r_1 a_2}_{a_1 b_1} - 2S^{s_1}_{a_2} S^{a_2}_{b_2} \tilde{v}^{r_1 b_2}_{a_1 b_1}$$
$$- 2S^{a_2}_{b_1} S^{b_2}_{a_2} \tilde{v}^{r_1 s_1}_{a_1 b_2} \Big] - 2t^{a_1 b_1}_{r_1 s_1} \Big[2S^{r_1}_{b_2} \tilde{v}^{b_2 s_1}_{a_1 b_1}$$
$$- 2S^{r_1}_{b_2} S^{b_2}_{a_2} \tilde{v}^{a_2 s_1}_{a_1 b_1} - 2S^{b_2}_{a_2} S^{r_1}_{b_1} \tilde{v}^{r_1 s_1}_{a_2 b_1} \Big]. \quad (48)$$

To explicitly show the origin of this savings, we first must recognize two useful intermediates that could be formed,

$$T^P_{a_1 r_1} = t^{a_1 b_1}_{r_1 s_1} B^P_{b_1 s_1} \approx -C^Q_{a_1 r_1} C^Q_{b_1 s_1} B^P_{b_1 s_1} d^L_{a_1 r_1} d^L_{b_1 s_1},$$
$$T^P_{b_1 s_1} = t^{a_1 b_1}_{r_1 s_1} A^P_{a_1 r_1} \approx -C^Q_{a_1 r_1} C^Q_{b_1 s_1} A^P_{a_1 r_1} d^L_{a_1 r_1} d^L_{b_1 s_1}. \quad (49)$$

This allows us to write

$$E^{(20)}_{exch-disp}(S^2)(\mathcal{L}) = -2T^P_{b_1 s_1} \Big[2S^{s_1}_{a_2} B^P_{a_2 b_1} - 2S^{s_1}_{a_2} S^{a_2}_{b_2} B^P_{b_1 b_2}$$
$$- 2S^{a_2}_{b_1} S^{b_2}_{a_2} B^P_{b_2 s_1} \Big] - 2T^P_{a_1 r_1} \Big[2S^{r_1}_{b_2} A^P_{a_1 b_2}$$
$$- 2S^{r_1}_{b_2} S^{b_2}_{a_2} A^P_{a_1 a_2} - 2S^{a_2}_{b_2} S^{b_2}_{a_1} A^P_{a_2 r_1} \Big]. \quad (50)$$

Using canonical energy denominators, the formation of these intermediates would scale $\mathcal{O}(o^2v^2N_{df})$; if the Laplace transform is applied to the energy denominator, this scaling can be reduced to $\mathcal{O}(ovN^2_{df})$. Once these intermediates are available, their contribution to $E^{(20)}_{exch-disp}$ can be evaluated simply by contracting the overlap integrals with the DF integrals that appear in a certain term and then multiplying by the appropriate T type intermediate.

The remaining terms can be reduced to a dispersion amplitude and two two-index arrays. Structurally, there are two types of these terms, $t^{a_1 b_1}_{r_1 s_1} X_{a_1 r_1} Y_{b_1 s_1}$ and $t^{a_1 b_1}_{r_1 s_1} X_{a_1 s_1} Y_{b_1 r_1}$. When the dispersion amplitudes are written with Laplace transformed energy denominators and DF integrals, the former can be evaluated with $\mathcal{O}(ovN_{df})$ work, whereas the latter can be evaluated with $\mathcal{O}(o^2vN_{df})$ work,

$$E^{(20)}_{exch-disp}(S^2)(N^3, N^4)$$
$$= -2t^{a_1 b_1}_{r_1 s_1} \Big[S^{s_1}_{a_1} \big(2\tilde{v}^{a_2 r_1}_{a_2 b_1} - \tilde{v}^{r_1 a_2}_{a_2 b_1} \big) + S^{r_1}_{b_1} \big(2\tilde{v}^{s_1 b_2}_{a_1 b_2} - \tilde{v}^{b_2 s_1}_{a_1 b_2} \big)$$
$$+ S^{r_1}_{b_1} S^{b_2}_{a_2} \tilde{v}^{a_2 s_1}_{a_1 b_2} - 2S^{r_1}_{b_1} S^{b_2}_{a_1} \tilde{v}^{a_2 s_1}_{a_2 b_2} + 4S^{r_1}_{b_2} S^{b_2}_{a_1} \tilde{v}^{a_2 s_1}_{a_2 b_1}$$
$$+ S^{s_1}_{a_1} S^{a_2}_{b_2} \tilde{v}^{r_1 b_2}_{a_2 b_1} - 2S^{s_1}_{a_1} S^{a_2}_{b_1} \tilde{v}^{r_1 b_2}_{a_2 b_2} + 4S^{s_1}_{a_2} S^{a_2}_{b_1} \tilde{v}^{r_1 b_2}_{a_1 b_2}$$
$$- 2S^{r_1}_{b_1} S^{s_1}_{a_2} \tilde{v}^{a_2 b_2}_{a_1 b_2} - 2S^{r_1}_{b_2} S^{s_1}_{a_1} \tilde{v}^{a_2 b_2}_{a_2 b_1} \Big]. \quad (51)$$

III. RESULTS AND DISCUSSION

A. Timings

Our previous implementation of DF-SAPT0 primarily used the DF approximation to avoid the two-electron integral AO to MO transformation.[34] Additionally, the DF integrals were used to factor one contribution to $E^{(20)}_{exch-disp}$ in which the *ovov* type integrals appear (this approach was described in Ref. 38). Despite this relatively simple approach, SAPT0 computations with as many as 116 atoms could be routinely performed with the program developed in Ref. 34. Unfortunately, this approach is not tractable for much larger systems. We will use the largest intercalator complex studied in this work as a concrete example of the deficiencies in our previous implementation. The solution of the CPHF equations in the MO basis involves iterative matrix-vector multiplies with a matrix that is $ov \times ov$. For the complex of proflavine with a CGA stretch of DNA (Pf · CGA), this matrix can become as large as 9.3 TB. The evaluation of the $E^{(20)}_{exch-disp}$ term could be written as a dot product between the dispersion amplitudes and a collection of integrals contracted with overlap integrals (see Eq. (44)). While this was done explicitly in our previous implementation, many of the contributions were evaluated as dot products between $ov \times ov$ matrices. The dispersion amplitudes can also become rather large, 650 GB or 1.3 TB for the Pf · CGA complex, depending on the use of the frozen core approximation. For the remaining exchange terms, even o^3v arrays can be as large as 250 GB.

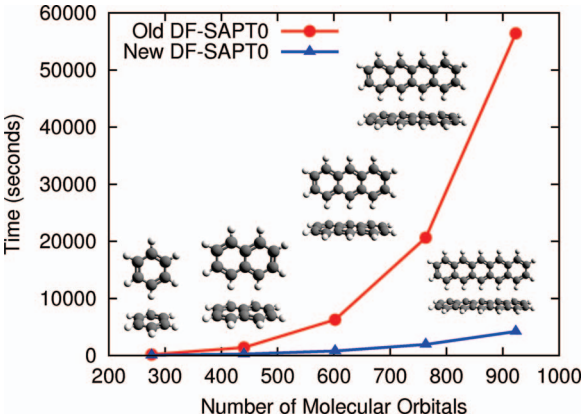

FIG. 1. Timings of SAPT0/aug-cc-pVDZ′ computations on T-shaped acenes, benzene through pentacene. The "Old DF-SAPT0" implementation is described in Ref. 34; the "New DF-SAPT0" implementation is described in the present work. These computations were performed on dual quad-core Intel Xeon processors clocked at 2.66 GHz. The energy denominators were approximated using Laplace transformation techniques with a threshold of 10^{-3}; this corresponds to 5 quadrature points for all five of the dimers.

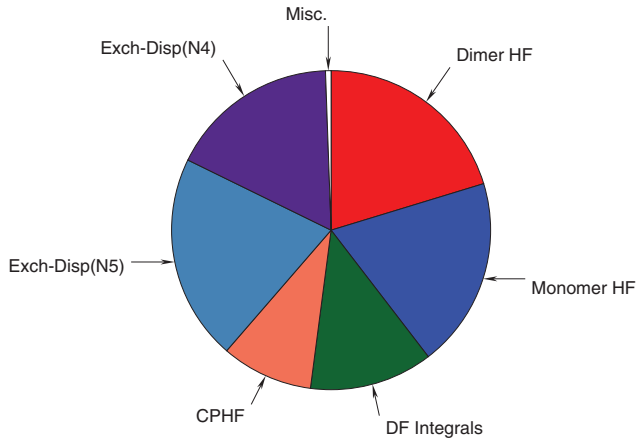

FIG. 2. Timing of a SAPT0/aug-cc-pVDZ′ computation on the Pf · CGA complex with 220 atoms and 2845 basis functions. The prerequisite mononer and dimer density-fitted Hartree-Fock computations required 40.4 h of total wall time. The SAPT0 computation required 61.7 h of total wall time. The total wall time for the complete computation was 102.1 h. These computations were performed on dual quad-core Intel Xeon processors clocked at 2.66 GHz.

Since our previous implementation was limited by the size of four-index arrays, the DF-SAPT0 algorithm developed in the present work minimizes the number of these arrays that must ever be formed. As a result, the new algorithm allows SAPT0 computations to be performed for much larger systems. Additionally, the factorization of the generalized two-electron integrals described above allows for increased efficiency with regard to memory usage; the evaluation of exchange terms can now be trivially blocked over the auxiliary index. Possibly the greatest advantage of our new implementation of SAPT0 is that the improvements in terms of tractability and memory efficiency does not come at the cost of performance. Figure 1 shows the timings for a series of T-shaped acenes (described in Ref. 34). For the largest system considered here, pentacene dimer, the new implementation of SAPT0 is over 12 times faster.

The advances described above have allowed the application of SAPT0 to large biological complexes. Here, we will highlight the Pf · CGA complex, which consists of 220 atoms and 2845 basis functions. This computation was performed using only modest computational resources: dual quad-core Intel Xeon processors clocked at 2.66 GHz, 40 GB of memory, and just over 4 days of total wall time. The underlying dimer and monomer density-fitted Hartree-Fock computations required a total of slightly over 1.5 days, with three-index integrals shared between the three computations. The subsequent SAPT0 computation required just over 2.5 days. Based on this performance, we estimate that our current DF-SAPT0 implementation should be scalable to 4000 basis functions. The relative expense of various parts of the computation on the Pf · CGA complex is shown in detail in Figure 2. The dimer and monomer density-fitted Hartree-Fock computations required approximately 40% of the total wall time. Of the remainder, the time of a SAPT0 computation is dominated by the evaluation of $E^{(20)}_{exch-disp}$, which requires nearly 2/3 of the total SAPT0 time. Here, we use the Laplace transform of the energy denominators with a threshold of 10^{-6}, which requires 10 quadrature points. The evaluation of the DF integrals (including formation of the AO integrals, multiplication by $[J_{AB}]^{-1/2}$, and AO to MO transformation) takes roughly 1/5 of the SAPT0 time, with the bulk of the remainder being spent in the solution of the CPHF equations. To improve efficiency in terms with heavy disk I/O requirements (the DF integrals and CPHF evaluation), the disk I/O is done asynchronously. In the CPHF equations, for example, reading of the $C^P_{r_1 r_2}$ DF integrals is "hidden" under the contractions described in Eq. (43). The remaining terms, $E^{(10)}_{elst}$, $E^{(10)}_{exch}$, etc., are trivial in comparison.

B. Accuracy of approximate energy denominators

The introduction of approximations to the energy denominator for a portion of the exchange-dispersion term introduces an additional source of error into the DF-SAPT0 ansatz. This error can be arbitrarily attenuated by refining the desired error criterion δ in the denominator decomposition, at the cost of a linear increase in computational expense with the number of Laplace quadrature points or Cholesky vectors. It is desirable to produce a single δ criterion that provides efficient computational performance and negligible numerical error for all systems. To achieve very small numerical errors is not at all demanding in this implementation: energy decompositions are only used to factor parts of the exchange-dispersion term, which is typically less than 10% of the size of the dispersion term. When the magnitude of the errors associated with the DF and frozen core approximations are considered, additional errors from the approximate energy denominators of less than one thousandth of one kcal mol^{-1} are easily acceptable in this term.

To benchmark the accuracy of Laplace and Cholesky decompositions of the energy denominator, we have computed error metrics for the $E^{(20)}_{exch-disp}$ term evaluated at a range of

TABLE I. Errors in the $E^{(20)}_{exch-disp}$ term evaluated with approximate energy denominators for the S22 test set.[12]

Laplace transform, aug-cc-pVDZ					
Threshold	10^{-2}	10^{-3}	10^{-4}	10^{-5}	10^{-6}
Points[a]	3.00	4.27	5.95	7.05	8.73
MSE[b]	-7.64×10^{-4}	1.36×10^{-5}	-7.00×10^{-6}	5.45×10^{-9}	-6.82×10^{-9}
MUE[c]	7.66×10^{-4}	9.16×10^{-5}	7.39×10^{-6}	4.94×10^{-7}	3.05×10^{-8}
RMS[d]	1.07×10^{-3}	1.62×10^{-4}	1.12×10^{-5}	7.38×10^{-7}	4.62×10^{-8}
Cholesky decomposition, aug-cc-pVDZ					
Threshold	10^{-2}	10^{-3}	10^{-4}	10^{-5}	10^{-6}
Points	3.00	5.00	6.23	7.73	9.27
MSE	-2.02×10^{-3}	1.39×10^{-5}	-2.05×10^{-6}	-3.89×10^{-7}	-3.18×10^{-9}
MUE	2.02×10^{-3}	1.40×10^{-5}	2.50×10^{-6}	3.89×10^{-7}	3.18×10^{-9}
RMS	2.55×10^{-3}	2.09×10^{-5}	4.05×10^{-6}	5.52×10^{-7}	5.64×10^{-9}
Laplace transform, aug-cc-pVTZ					
Threshold	10^{-2}	10^{-3}	10^{-4}	10^{-5}	10^{-6}
Points	3.18	5.00	6.18	7.95	9.95
MSE	-8.50×10^{-4}	6.39×10^{-5}	2.29×10^{-6}	-1.29×10^{-7}	-7.73×10^{-9}
MUE	1.17×10^{-3}	7.77×10^{-5}	8.73×10^{-6}	5.60×10^{-7}	1.95×10^{-8}
RMS	1.63×10^{-3}	1.12×10^{-4}	1.33×10^{-5}	8.99×10^{-7}	3.13×10^{-8}
Cholesky decomposition, aug-cc-pVTZ					
Threshold	10^{-2}	10^{-3}	10^{-4}	10^{-5}	10^{-6}
Points	3.00	5.00	6.95	8.50	10.45
MSE	-1.97×10^{-3}	2.37×10^{-5}	-1.47×10^{-6}	-2.65×10^{-7}	3.18×10^{-9}
MUE	1.97×10^{-3}	2.38×10^{-5}	2.46×10^{-6}	3.11×10^{-7}	3.18×10^{-9}
RMS	2.49×10^{-3}	3.84×10^{-5}	3.93×10^{-6}	4.20×10^{-7}	7.69×10^{-9}

[a]Average number of quadrature points or average number of Cholesky vectors needed to obtain the specified accuracy (in a.u.).
[b]Mean signed error in kcal mol^{-1}.
[c]Mean unsigned error in kcal mol^{-1}.
[d]Root mean square error in kcal mol^{-1}.

δ over the S22 test set,[12] using the aug-cc-pVDZ and aug-cc-pVTZ basis sets. The core orbitals were frozen in all cases, and the results were compared against the exact DF-SAPT0 values within the same auxiliary basis. The results of this study are shown in Table I. Cholesky and Laplace show the same general trends: decreasing the δ parameter by one order of magnitude corresponds to a one to two order of magnitude decrease in error in the $E^{(20)}_{exch-disp}$ term, concomitant with an increase of one to two quadrature points or Cholesky vectors. Increasing basis size from aug-cc-pVDZ to aug-cc-pVTZ increases the HUMO energy, and thereby the intrinsic range R, inducing an increase of one quadrature point of Cholesky vector for some systems. For each value of δ and basis set, the Laplace approach requires one less quadrature point than Cholesky for a few systems. However, for a δ of 10^{-3}, the RMS error of Laplace decomposition is almost one order of magnitude larger than the equivalent Cholesky decomposition, but still far smaller than the required 10^{-3} kcal mol^{-1} accuracy. For all other values of δ, Cholesky and Laplace give almost identical accuracy. The outlier at a δ of 10^{-3} is probably due to the windowed nature of the quadratures supplied by Hackbusch, which were provided at discrete ranges of R. The quadratures could be refined for each problem by application of the minimax algorithm for the explicit value of R intrinsic to each system. We elected to not implement the minimax algorithm on the grounds that this refinement would save at most one quadrature point, and then only under certain circumstances. The slightly smaller number of quadrature points for each δ and the possibility of slight additional refinement point to Laplace decomposition being marginally more efficient than Cholesky decomposition; however, the difference is so slight as to be negligible from a computational standpoint. Laplace decomposition does provide the theoretical advantage that the factors are strictly positive, allowing for symmetric factorizations to take advantage of the ability to take the square roots of the Laplace factors. We have therefore elected to default to Laplace decomposition using the predetermined Hackbusch quadratures, and recommend a δ of 10^{-3}, which should result in errors of less than one part in one thousand in the $E^{(20)}_{exch-disp}$ term for all systems. This choice should result in a computationally efficient 4–5 quadrature points for most systems.

C. Application to intercalator complexes

The intercalation of DNA by proflavine has been a target of several previous theoretical studies. Langner *et al*. performed small-basis MP2 computations on neutral and protonated complexes of proflavine with A-U and C-G base pairs.[17] Additionally, they reported an energy decomposition for these complexes, based on partitioning of the MP2 interaction energy. More recently, Li *et al*. applied van der Waals DFT to the stacking of proflavine on C-G and T-A base pairs.[20]

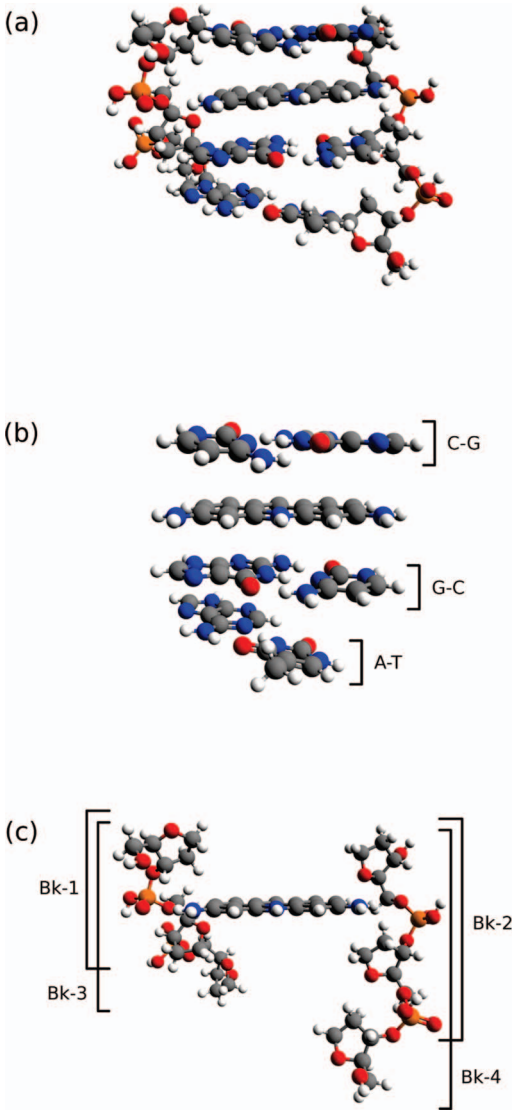

FIG. 3. Geometries of proflavine intercalation complexes studied in this work. (a) Proflavine intercalating a CG step. Complexes including the CG and CGA segments of DNA are studied. (b) Three geometries of proflavine interacting with individual base pair duplexes. (c) Four geometries of proflavine interacting with segments of the DNA backbone.

Unfortunately, neither of these studies include the backbone in their computations. This is consistent with other quantum mechanical studies on intercalation (involving other intercalating molecules).[15,16,19,68] In order to determine the importance of the backbone in the intercalation of DNA, lower-scaling methods must be applied. Our implementation of DF-SAPT0 allows intercalation phenomena to be probed at semi-quantitative accuracy without neglecting backbone and neighboring base pair interactions.

In this work, we will consider the intercalation of a CG step by a protonated, cationic proflavine molecule; in Figure 3(a), the geometry considered is shown. An AT base pair neighbors the intercalation site (the full segment of DNA will be denoted with its sequence, CGA). This geometry is taken from a crystal structure[69] with the hydrogen positions determined by constrained B3LYP/6-31G** optimization. The effect of solution-phase cations (e.g., Na^+, K^+) that interact with the anionic phosphates in the backbone is mimicked by protonating the backbone to obtain a neutral species. In addition to considering the interaction between proflavine and the full trinucleotide duplex, the complex is fragmented into various model systems. The fragmentation into base pair-proflavine interactions is shown in Figure 3(b) and the fragmentation into backbone-proflavine interactions is shown in Figure 3(c). Any covalent bonds cut during the fragmentation are capped with hydrogen atoms whose positions are determined by B3LYP/6-31G** optimization. While it is straightforward to isolate the effect of the neighboring (AT) base pair, it is difficult to fragment the backbone in a manner that isolates its neighboring portion. For this reason, we will consider the portion of the backbone that is adjacent to the intercalation site and the entire backbone; the differences between the interaction of these fragments with proflavine will provide insight into the role of the neighboring portion of the backbone.

First, we will consider the interaction of proflavine with the local portion of the intercalation site. The results from the DF-SAPT0 computations can be found in Table II. In the following discussion, we will refer to the designation of intermolecular interactions as electrostatics-dominated, dispersion-dominated, or mixed-influence based on the metric used by Hobza and co-workers:[70] if an interaction contains twice as much dispersion as electrostatics, then it is dispersion dominated (and vice versa); otherwise, it is designated as a mixed influence interaction. Using this definition, the interaction of proflavine with the CG step should be described as a mixed-influence interaction. One interpretation of this result might involve the nature of catonic π-π stacking interactions present in this complex. While retaining the strong dispersion interactions found in neutral π-π interactions, catonic π-π interactions should have enhanced electrostatic and induction interactions. The SAPT compuations of the Pf · C-G and Pf · G-C base pair-proflavine interactions show that, indeed, there are significant electrostatic contributions from the stacking of the cationic proflavine intercalator. However, they also indicate that the dispersion contributions are more than twice as large. Perhaps surprisingly, more than a third of the electrostatic contribution in the whole intercalator complex comes from intercalator-backbone contributions. In fact, the intecalator-backbone interaction contributes about one third of the overall SAPT0 interaction energy of the complex.

Careful examination of the Pf · CG geometry reveals that the proflavine favors one side of the complex and forms two long hydrogen bonds with the phosphate group. One contact is between the terminal NH_2 group and a phosphate oxygen (2.64 Å), and the other is between an aromatic hydrogen and another phosphate oxygen (2.52 Å). The NH · · · O and CH · · · O contacts are both nearly linear (178.4° and 176.3°, respectively). (There is also at least one favorable aromatic CH · · · O contact with a sugar oxygen on the other backbone strand, at a distance of 2.59 Å, but this one occurs at an angle of 135° instead of the favored linear arrangement). The presence of the two long hydrogen bonds appears in the SAPT computations of the Pf · Bk-1 interaction (see Figure 3(c) for the definition of the various backbone fragments considered); this interaction, although designated as mixed influence due

TABLE II. SAPT0/aug-cc-pVDZ′ computations of complexes of proflavine with a CGA segment of DNA and fragments of the DNA segment, energies in kcal mol^{-1}.

	E_{elst}	E_{exch}	E_{ind}	E_{disp}	E_{SAPT0}
Proflavine · DNA					
Pf · CG	− 38.8	54.1	− 10.4	− 66.0	− 61.1
Pf · CGA	− 37.9	54.2	− 11.4	− 67.6	− 62.7
Proflavine base pair					
Pf · C-G	− 11.2	22.4	− 3.9	− 26.1	− 18.8
Pf · G-C	− 13.0	22.6	− 4.0	− 26.8	− 21.2
Pf · A-T	− 1.3	0.0	− 0.3	− 0.7	− 2.3
Proflavine backbone					
Pf · Bk-1	− 12.2	6.8	− 3.0	− 7.6	− 16.0
Pf · Bk-2	− 3.3	3.6	− 1.8	− 4.9	− 6.5
Pf · Bk-3	− 13.2	6.8	− 3.2	− 7.7	− 17.3
Pf · Bk-4	− 0.3	3.6	− 1.9	− 5.1	− 3.7
Fragmented proflavine · CG					
s(Pf · CG)[a]	− 24.2	45.0	− 7.9	− 52.9	− 40.0
b(Pf · CG)[b]	− 15.6	10.4	− 4.8	− 12.5	− 22.5
(Pf · CG)[c]	− 39.8	55.4	− 12.8	− 65.4	− 62.5
Fragmented proflavine · CGA					
s(Pf · CGA)[a]	− 25.5	45.0	− 8.3	− 53.6	− 42.3
b(Pf · CGA)[b]	− 13.5	10.4	− 5.1	− 12.8	− 21.0
(Pf · CGA)[c]	− 39.0	55.4	− 13.4	− 66.3	− 63.3

[a]Interaction due to stacking of proflavine with base pairs.
[b]Interaction of proflavine with the DNA backbone.
[c]Interaction of proflavine with the segment of DNA computed as a sum of fragments.

to significant long-range dispersion, contains a very strong electrostatic component. The interaction with the other backbone (the Pf · Bk-2 interaction), to which the proflavine does not from a hydrogen bond, is much weaker and less electrostatic in nature. The importance of the proflavine-backbone interactions suggest that they must be included in future studies. The geometric dependence of hydrogen bonding interactions makes it crucial to obtain reasonable geometries for intercalator-DNA complexes if the intercalator-backbone interactions are to be reasonably described. While scans of the intercalator-base pair potential energy surface are interesting insofar as they provide insight into the nature of the stacking interaction, these types of studies do not capture many of the important contributions to the complex geometry. Even though the stacking interaction comprises two-thirds of the total interaction, stacking potential energy surfaces are usually flat compared to a hydrogen bonded surface; therefore, the complex geometry may be significantly influenced by intercalator-backbone interactions.

Our new SAPT0 implementation is also efficient enough to allow examination of the interactions between the intercalator and a neighboring base pair. The Pf · CGA interaction energy differs from the Pf · CG interaction energy by less than 3%. The inclusion of the neighboring base pair adds some additional long-range dispersion, a slightly increased induction interaction, and a weakly repulsive electrostatic interaction. As revealed by SAPT0 computations on the Pf · AT complex, the additional dispersion interactions (as well as an attractive electrostatic contribution) can be attributed, mainly, to the distant Pf · A-T stacking. The source of the repulsive electrostatic contribution between proflavine and the neighboring part of the DNA trimer appears to be an unfavorable configuration of the additional proflavine-sugar contact. Overall, it does not appear that neighboring base pairs play an important role in the energetics or geometry of an intercalator-DNA complex (unless, perhaps, the intercalator is much larger than proflavine).

IV. CONCLUSIONS

Zeroth-order symmetry-adapted perturbation theory (SAPT0) has the attractive property of providing semiquantitative insight into the nature of molecular interactions at relatively low computational expense. The application of density fitting (DF) approximations and Laplace transformation techniques allows for new factorizations of the SAPT0 energy equations. The use of dressed DF two-electron integrals allows the generalized two-electron integrals, which appear in SAPT exchange corrections, to be written in terms of three-index arrays. This provides new possibilities for the factorization of the SAPT0 exchange terms. The use of DF integrals allows the CPHF equations to be efficiently evaluated in the MO basis with reduced disk I/O. Finally, the Laplace transformation techniques remove the disk I/O (or redundant computation) associated with the dispersion amplitudes that had previously limited the applicability of SAPT0, including DF-SAPT0. As there are several approximate techniques for treating energy denominators, we have tested the quadratures developed by Braess and Hackbusch[42,43] for the Laplace transformation of the energy denominator against partial Cholesky decomposition and determined the the Laplace transformation requires, on average, fewer quadrature points to approximate the energy denominator. With roughly 4–5 quadrature points, errors due to the approximation of the energy denominator of less than 10^{-4} kcal mol^{-1} can be obtained in SAPT0 energies for the S22 test set.[12] These advances offer a significant improvement over previous implementations of SAPT0 and allow these computations to be performed on systems with more than 200 atoms and 2800 basis functions. It is estimated that the implementation of DF-SAPT0 reported in this work should be applicable to systems with 4000 basis functions.

The common feature of all approximations used within this work is that they are both generic and controllable. The former means that the efficient application of the approximation does not depend on the particular electronic environment or spatial extent of the chemical system. The latter implies that an arbitrary level of accuracy can be obtained within the SAPT0 ansatz by increasing the δ parameter for energy denominator decomposition or the completeness of the auxiliary basis set for the two-electron integrals. If extrinsic assumptions of large system size and sparseness of the density matrix are applied, linear scaling algorithms could be developed for the entirety of SAPT0, e.g., based on the methods of Ochsenfeld *et al.*[71,72]

DF-SAPT0 computations on the complex of a DNA sequence (CGA) with protonated proflavine have been performed to elucidate the nature of intercalation phenomena. Owing to the scalability of our new DF-SAPT0

implementation, the entire proflavine-CGA complex can be examined, including all three base pairs and the backbone atoms. The stacking interactions comprise two-thirds of the total, while the proflavine-backbone interactions account for the remaining third. Overall, the interaction contains important contributions from electrostatics and dispersion; however, the dispersion interactions are mainly due to stacking interactions, while a significant fraction of the electrostatic interaction is a result of proflavine forming long hydrogen bonds with the backbone. Such hydrogen bonding contacts are likely to influence the intercalation geometry. Although the energetics of the complex are largely comprised of cationic π-π stacking interactions, these interactions should be less sensitive to the geometry of the complex than intercalator-backbone hydrogen bonds would be, likely magnifying the importance of the latter in influencing the intercalation geometry. Future studies of intercalation phenomena should include intercalator-backbone interactions and their geometric implications. Efficient implementations of reliable computational methods are essential for the study of large biologically relevant molecules; we have demonstrated that DF-SAPT0 is now capable of providing unique insight into these types of systems.

ACKNOWLEDGMENTS

We thank Professors Nicholas Hud and Loren Williams for providing the crystal structure for the proflavine intercalation complex. This material is based upon work supported by the National Science Foundation through grants to C.D.S. (Grant No. CHE-1011360) and H.F.S. (Grant No. CHE-1054286). The Center for Computational Molecular Science and Technology is funded through an NSF CRIF award (Grant No. CHE-0946869) and by Georgia Tech.

[1] J. C. Collings, K. P. Roscoe, E. G. Robins, A. S. Batsanov, L. M. Stimson, J. A. K. Howard, S. J. Clark, and T. B. Marder, New J. Chem. **26**, 1740 (2002).
[2] A. L. Ringer and C. D. Sherrill, Chem. Eur. J. **14**, 2542 (2008).
[3] R. Podeszwa, B. M. Rice, and K. Szalewicz, Phys. Rev. Lett. **101**, 115503 (2008).
[4] R. Podeszwa, B. M. Rice, and K. Szalewicz, Phys. Chem. Chem. Phys. **11**, 5512 (2009).
[5] H.-S. Shieh, H. M. Berman, M. Dabrow, and S. Neidle, Nucleic Acids Res. **8**, 85 (1980).
[6] W. Saenger, *Principles of Nucleic Acid Structure* (Springer-Verlag, New York, 1984).
[7] S. K. Burley and G. A. Petsko, Science **229**, 23 (1985).
[8] J. Šponer, J. Leszczynski, and P. Hobza, J. Phys. Chem. **100**, 5590 (1996).
[9] M. Elstner, P. Hobza, T. Frauenheim, S. Suhai, and E. Kaxiras, J. Chem. Phys. **114**, 5149 (2001).
[10] P. Jurečka and P. Hobza, J. Am. Chem. Soc. **125**, 15608 (2003).
[11] E. A. Meyer, R. K. Castellano, and F. Diederich, Angew. Chem., Int. Ed. **42**, 1210 (2003).
[12] P. Jurečka, J. Šponer, J. Černý, and P. Hobza, Phys. Chem. Chem. Phys. **8**, 1985 (2006).
[13] A. L. Ringer, M. S. Figgs, M. O. Sinnokrot, and C. D. Sherrill, J. Phys. Chem. A **110**, 10822 (2006).
[14] A. L. Ringer, A. Senenko, and C. D. Sherrill, Protein Sci. **16**, 2216 (2007).
[15] D. A. Bondarev, W. J. Skawinski, and C. A. Venanzi, J. Phys. Chem. B **104**, 815 (2000).
[16] A. Kumar, M. Elstner, and S. Suhai, Int. J. Quantum Chem. **95**, 44 (2003).
[17] K. M. Langner, P. Kedzierski, W. A. Sokalski, and J. Leszczynski, J. Phys. Chem. B **110**, 9720 (2006).
[18] D. L. Mobley, A. P. Graves, J. D. Chodera, A. C. McReynolds, B. K. Shoichet, and K. A. Dill, J. Mol. Biol. **371**, 1118 (2007).
[19] J. G. Hill and J. A. Platts, Chem. Phys. Lett. **479**, 279 (2009).
[20] S. Li, V. R. Cooper, T. Thonhauser, B. I. Lundqvist, and D. C. Langreth, J. Phys. Chem. B **113**, 11166 (2009).
[21] M. Kolář, T. Kubař, and P. Hobza, J. Phys. Chem. B **114**, 13446 (2010).
[22] J. C. Faver, M. L. Benson, X. He, B. P. Roberts, B. Wang, M. S. Marshall, M. R. Kennedy, C. D. Sherrill, and K. M. Merz, J. Chem. Theory Comput. **7**, 790 (2011).
[23] K. Morokuma, J. Chem. Phys. **55**, 1236 (1971).
[24] K. Kitaura and K. Morokuma, Int. J. Quantum Chem. **10**, 325 (1976).
[25] P. S. Bagus, K. Hermann, and C. W. Bauschlicher, J. Chem. Phys. **80**, 4378 (1984).
[26] W. Stevens and W. Fink, Chem. Phys. Lett. **139**, 15 (1987).
[27] B. Jeziorski, R. Moszynski, and K. Szalewicz, Chem. Rev. **94**, 1887 (1994).
[28] W. Chen and M. S. Gordon, J. Phys. Chem. **100**, 14316 (1996).
[29] H. L. Williams and C. F. Chabalowski, J. Phys. Chem. A **105**, 646 (2001).
[30] A. J. Misquitta and K. Szalewicz, Chem. Phys. Lett. **357**, 301 (2002).
[31] A. J. Misquitta, B. Jeziorski, and K. Szalewicz, Phys. Rev. Lett. **91**, 033201 (2003).
[32] A. Heßelmann and G. Jansen, Phys. Chem. Chem. Phys. **5**, 5010 (2003).
[33] A. J. Misquitta, R. Podeszwa, B. Jeziorski, and K. Szalewicz, J. Chem. Phys. **123**, 214103 (2005).
[34] E. G. Hohenstein and C. D. Sherrill, J. Chem. Phys. **132**, 184111 (2010).
[35] E. G. Hohenstein and C. D. Sherrill, J. Chem. Phys. **133**, 014101 (2010).
[36] E. G. Hohenstein and C. D. Sherrill, J. Chem. Phys. **133**, 104107 (2010).
[37] R. Bukowski, R. Podeszwa, and K. Szalewicz, Chem. Phys. Lett. **414**, 111 (2005).
[38] A. Heßelmann, G. Jansen, and M. Schütz, J. Chem. Phys. **122**, 014103 (2005).
[39] R. Podeszwa, R. Bukowski, and K. Szalewicz, J. Chem. Theory Comput. **2**, 400 (2006).
[40] J. Almlöf, Chem. Phys. Lett. **181**, 319 (1991).
[41] M. Häser and J. Almlöf, J. Chem. Phys. **96**, 489 (1992).
[42] D. Braess and W. Hackbusch, IMA J. Numer. Anal. **25**, 685 (2005).
[43] A. Takatsuka, S. Ten-no, and W. Hackbusch, J. Chem. Phys. **129**, 044112 (2008).
[44] J. L. Whitten, J. Chem. Phys. **58**, 4496 (1973).
[45] B. I. Dunlap, J. W. D. Connolly, and J. R. Sabin, Int. J. Quantum Chem. Symp. **11**, 81 (1977).
[46] B. I. Dunlap, J. W. D. Connolly, and J. R. Sabin, J. Chem. Phys. **71**, 3396 (1979).
[47] O. Vahtras, J. Almlöf, and M. W. Feyereisen, Chem. Phys. Lett. **213**, 514 (1993).
[48] M. Feyereisen, G. Fitzgerald, and A. Komornicki, Chem. Phys. Lett. **208**, 359 (1993).
[49] A. P. Rendell and T. J. Lee, J. Chem. Phys. **101**, 400 (1994).
[50] F. Weigend, Phys. Chem. Chem. Phys. **4**, 4285 (2002).
[51] H.-J. Werner, F. R. Manby, and P. J. Knowles, J. Chem. Phys. **118**, 8149 (2003).
[52] H. Koch and A. S. de Merás, J. Chem. Phys. **113**, 508 (2000).
[53] J. M. Turney, A. C. Simmonett, R. M. Parrish, E. G. Hohenstein, F. Evangelista, J. T. Fermann, B. J. Mintz, L. A. Burns, J. J. Wilke, M. L. Abrams, N. J. Russ, M. L. Leininger, C. L. Janssen, E. T. Seidl, W. D. Allen, H. F. Schaefer, R. A. King, E. F. Valeev, C. D. Sherrill, and T. D. Crawford, "PSI4: An open-source *ab initio* electronic structure program," WIREs Comput. Mol. Sci. (in press).
[54] B. Jeziorski, M. Bulski, and L. Piela, Int. J. Quantum Chem. **10**, 281 (1976).
[55] R. Moszynski, T. G. A. Heijmen, and B. Jeziorski, Mol. Phys. **88**, 741 (1996).
[56] T. H. Dunning, J. Chem. Phys. **90**, 1007 (1989).
[57] R. A. Kendall, T. H. Dunning, and R. J. Harrison, J. Chem. Phys. **96**, 6796 (1992).
[58] N. H. F. Beebe and J. Linderberg, Int. J. Quantum Chem. **12**, 683 (1977).
[59] I. Roeggen and E. Wisloff-Nilssen, Chem. Phys. Lett. **132**, 154 (1986).
[60] H. Koch, A. S. de Meras, and T. B. Pedersen, J. Chem. Phys. **118**, 9481 (2003).
[61] F. Aquilante, T. B. Pedersen, and R. Lindh, J. Chem. Phys. **126**, 194106 (2007).
[62] F. Weigend, A. Köhn, and C. Hättig, J. Chem. Phys. **116**, 3175 (2002).
[63] Y. Jung, R. C. Lochan, A. D. Dutoi, and M. Head-Gordon, J. Chem. Phys. **121**, 9793 (2004).

[64]R. Moszynski, B. Jeziorski, and K. Szalewicz, J. Chem. Phys. **100**, 1312 (1994).
[65]R. Moszynski, B. Jeziorski, S. Rybak, K. Szalewicz, and H. L. Williams, J. Chem. Phys. **100**, 5080 (1994).
[66]B. Jeziorski, R. Moszynski, A. Ratkiewicz, S. Rybak, K. Szalewicz, and H. L. Williams, in *Methods and Techniques in Computational Chemistry: METECC94*, edited by E. Clementi, Vol. B (Medium-Size Systems) (STEF, Cagliari, 1993), p. 79.
[67]R. Bukowski, W. Cencek, K. Patkowski, P. Jankowski, M. Jeziorska, M. Kolaski, and K. Szalewicz, Mol. Phys. **104**, 2241 (2006).
[68]D. Řeha, M. Kabeláč, F. Ryjáček, J. Šponer, J. E. Šponer, M. Elstner, S. Suhai, and P. Hobza, J. Am. Chem. Soc. **124**, 3366 (2002).
[69]T. Maehigashi, O. Persil, N. V. Hud, and L. D. Williams, unpublished results, nucleic acid database (NDB) ID DD0103.
[70]L. Gráfová, M. Pitoňák, J. Řezáč, and P. Hobza, J. Chem. Theory Comput. **6**, 2365 (2010).
[71]B. Doser, D. S. Lambrecht, J. Kussmann, and C. Ochsenfeld, J. Chem. Phys. **130**, 064107 (2009).
[72]M. Beer and C. Ochsenfeld, J. Chem. Phys. **128**, 221102 (2008).